Monolayer coverage and channel length set the mobility in self-assembled monolayer field-effect transistors

Mathijssen, Simon G. J.; Smits, Edsger C. P.; van Hal, Paul A.; Wondergem, Harry J.; Ponomarenko, Sergei A.; Moser, Armin; Resel, Roland; Bobbert, Peter A.; Kemerink, Martijn; Janssen, Rene A. J.

Published in:
Nature Nanotechnology

DOI:
10.1038/nnano.2009.201

Publication date:
2009

ARTICLES
PUBLISHED ONLINE: 9 AUGUST 2009 | DOI: 10.1038/NNANO.2009.201
nature nanotechnology

Monolayer coverage and channel length set the mobility in self-assembled monolayer field-effect transistors

Simon G. J. Mathijssen[1,2], Edsger C. P. Smits[1,3], Paul A. van Hal[1], Harry J. Wondergem[1], Sergei A. Ponomarenko[4], Armin Moser[5], Roland Resel[5], Peter A. Bobbert[2], Martijn Kemerink[2], René A. J. Janssen[2] and Dago M. de Leeuw[1,6]*

The mobility of self-assembled monolayer field-effect transistors (SAMFETs) traditionally decreases dramatically with increasing channel length. Recently, however, SAMFETs using liquid-crystalline molecules have been shown to have bulk-like mobilities that are virtually independent of channel length. Here, we reconcile these scaling relations by showing that the mobility in liquid crystalline SAMFETs depends exponentially on the channel length only when the monolayer is incomplete. We explain this dependence both numerically and analytically, and show that charge transport is not affected by carrier injection, grain boundaries or conducting island size. At partial coverage, that is when the monolayer is incomplete, liquid-crystalline SAMFETs thus form a unique model system to study size-dependent conductance originating from charge percolation in two dimensions.

Charge carriers in a field-effect transistor are injected from the source contact, transported through the semiconductor, then collected at the drain contact. The carriers are confined by the gate field as a thin accumulation layer at the semiconductor–gate dielectric interface[1]. In a monolayer transistor the semiconductor consists of only a single sheet of molecules, and the layer thickness is comparable to that of the accumulation layer. Electrical transport is then, by definition, two-dimensional, so any structural imperfections such as voids or grain boundaries lead to potential barriers and, hence, to a deterioration in charge carrier mobility[2,3]. A prerequisite for efficient charge transport is long-range connectivity, and to form a conducting path between the source and drain electrode, the molecules should be intimately connected. In addition, the nature of the electrical contact is crucial. Historically, connecting an effective injecting electrode to a single layer of molecules has proven to be a challenge[4], and the extracted mobility in monolayer transistors is often orders of magnitude lower than that in corresponding bulk thin-film transistors due to injection-limited contacts[5–7].

Self-assembled[8] monolayer transistors in which the semiconductor is a monolayer spontaneously formed on the gate dielectric, traditionally show inverse scaling; that is, device mobility decreases dramatically with increasing channel length. Only sub-micrometre channels have shown a gate-dependent source–drain current, with the mobility in longer channels being negligible[4]. Recently, however, we have demonstrated self-assembled monolayer field-effect transistors (SAMFETs) in which the extracted device mobility is virtually independent of channel length[9]. To investigate this contradiction in the scaling of the mobility, we present a technology to fabricate SAMFETs with varying monolayer coverage and channel lengths. By ensuring both proper charge carrier injection and an ordered SAM microstructure, this technology allows the charge transport in a two-dimensional percolating semiconductor network to be systematically probed. For sub-monolayer coverage, the anomalous inverse scaling behaviour reported previously for SAMFETs is reproduced and can be accounted for by numerical and analytical percolation models.

SAMFETs[9] of varying coverage were prepared on heavily doped silicon wafers (acting as the common gate) covered with a 200-nm layer of thermally grown SiO_2. The gold source and drain contacts were defined by conventional photolithography and wet etchant chemistry. Titanium (10 nm) was used as an adhesion layer. The liquid-crystalline active molecule comprised a mesogenic quinquethiophene core, end-capped with an ethyl group to enhance stability and solubility. To bind the molecule to the SiO_2 gate dielectric, a monochlorosilane anchoring group was attached via an undecane spacer. The chemical structure of the self-assembling molecule, chloro[11-(5′′′′-ethyl-2,2′:5′,2′′:5′′,2′′′:5′′′,2′′′′-quinquethien-5-yl) undecyl]-dimethylsilane is shown in the inset to Fig. 1. To induce self-assembly of the molecules, the SiO_2 gate dielectric was activated by an oxygen plasma treatment followed by acid hydrolysis. The SAM was then formed by submerging the substrate in a dry toluene solution of the semiconducting molecule. The coverage was varied by changing the immersion time in the solution from 15 min to 30 min, 1 h and 15 h.

Typical topography images ($20 \times 20\ \mu m^2$) are presented in Fig. 1a–d. It is clear that the SAM grows in the form of islands, with coverage varying from 0.05 ± 0.05, 0.31 ± 0.08, 0.5 ± 0.1 to 1, respectively, depending on the immersion time. Note that the height difference in the topography is 3.5 nm, in perfect agreement with the calculated length of the molecule. A small fraction of the monolayer is a bilayer, most likely due to the formation of dimers in the solution.

[1]Philips Research Laboratories, High Tech Campus 4, 5656 AE Eindhoven, The Netherlands, [2]Department of Applied Physics, Eindhoven University of Technology, PO Box 513, 5600 MB Eindhoven, The Netherlands, [3]Holst Centre/TNO, High Tech Campus 34, 5656 AE Eindhoven, The Netherlands, [4]Enikolopov Institute of Synthetic Polymer Materials of Russian Academy of Sciences, Profsoyuznaya 70, 117393 Moscow, Russia, [5]Institute of Solid State Physics, Graz University of Technology, Petersgasse 16A, 8010 Graz, Austria, [6]Molecular Electronics, Zernike Institute for Advanced Materials, University of Groningen, Nijenborgh 4, 9747 AG Groningen, The Netherlands. *e-mail: dago.de.leeuw@philips.com

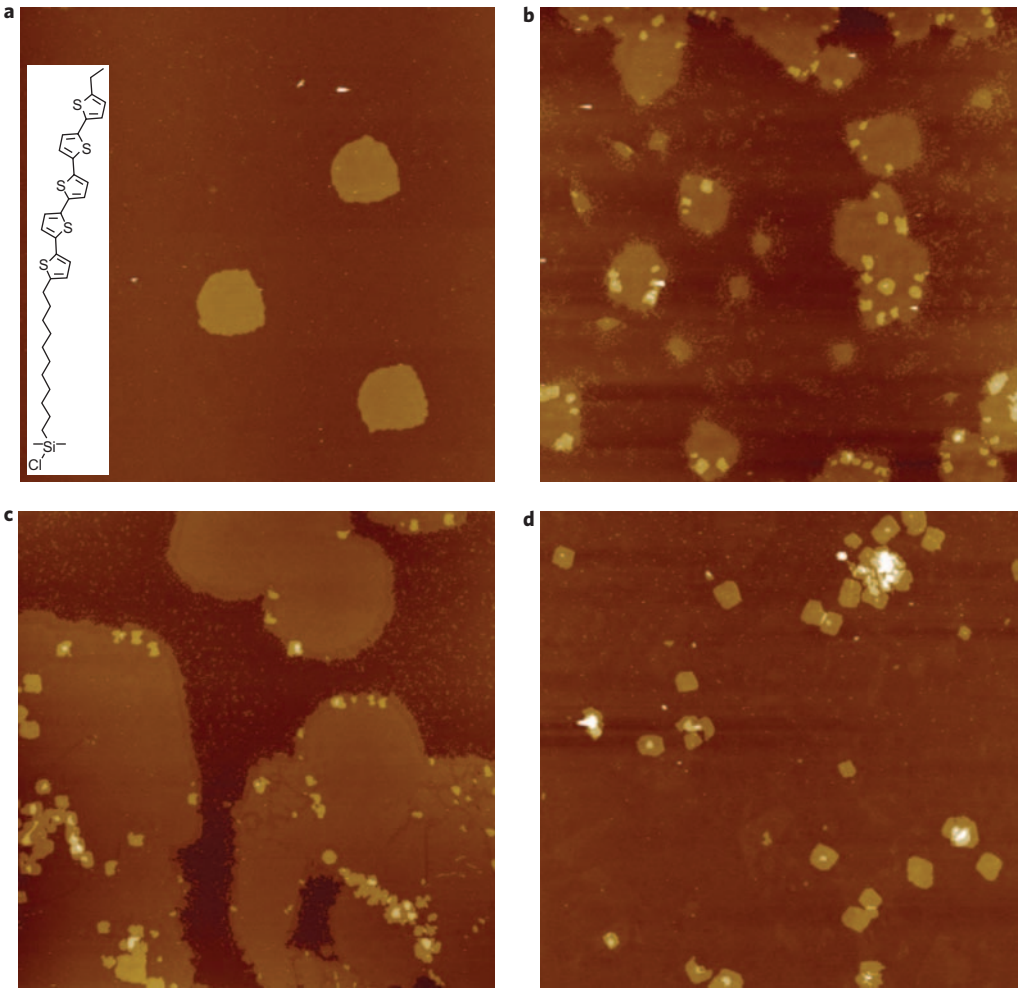

Figure 1 | SAM growth. a–d, Typical topography images ($20 \times 20\ \mu m^2$) of partially covered SAMFETs measured with AFM. The immersion time was varied from 15 min (**a**) to 30 min (**b**), 1 h (**c**) and 15 h (**d**), with coverage obtained as average values over six measurements, and equalling 0.05 ± 0.05, 0.31 ± 0.08, 0.5 ± 0.1 and 1, respectively. The inset to **a** shows the chemical structure of the self-assembling molecule.

A prerequisite to transport charges in self-assembled monolayers is long-range order. Self-assembled monolayers of alkanethiols on gold grow dynamically, and a perfectly ordered SAM is only obtained when the coverage is close to 100% (ref. 10). In contrast to alkanethiol monolayer formation on gold, the assembly of silanes on SiO_2 is far less reversible and the SAM grows through the development of islands[11]. In the present case, the self-assembling molecule consists of an aliphatic chain and a thiophene core, each having the capability to drive the self-assembly process. To obtain efficient charge transport, the thiophene units should be long-range ordered. The microstructure of the partially covered SAMs was determined from grazing incidence diffraction measurements. The diffracted intensity is presented as a colour map in Fig. 2 as a function of perpendicular and in-plane scattering vectors, q_z and q_{xy}. The horizontal line at low q_z is due to diffuse scattering from the sample surface at the critical angle as described by others[12]. Most important are the vertical lines, the so-called Bragg rods. They demonstrate in-plane order arising from the thiophene units; the rod shape results from the absence of periodicity perpendicular to the islands. The onset of the Bragg rods directly at the Yoneda line reveals that the thiophene units are oriented perpendicular to the substrate surface and packed in a herringbone structure (see Supplementary Information). The grazing incidence diffraction measurements show that the SAM grows in long-range ordered, crystalline islands.

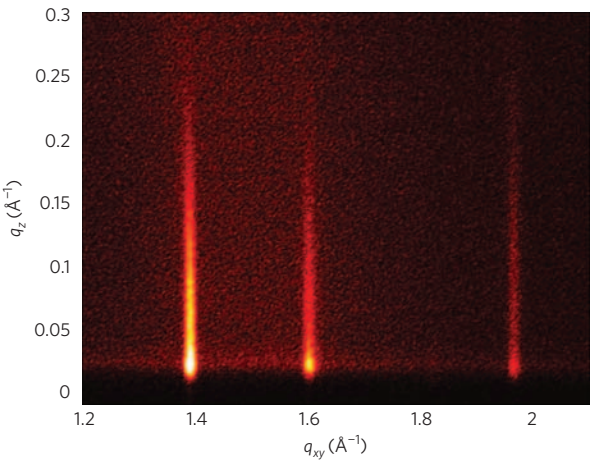

Figure 2 | SAM microstructure. Diffraction pattern from a partially covered SAM obtained with grazing incidence X-ray diffraction measurements. The diffracted intensity is presented as a function of the out-of-plane and in-plane scattering vectors q_z and q_{xy}. The Bragg rods at in-plane scattering vectors of 1.393, 1.605 and 1.968 Å^{-1} indicate an in-plane crystalline order within the islands of the incomplete SAM. The rods can be indexed as the (1.1), (0.2) and (1.2) reflections of a rectangular unit cell with lattice constants of 5.49 and 7.83 Å, demonstrating order in the partially covered SAM.

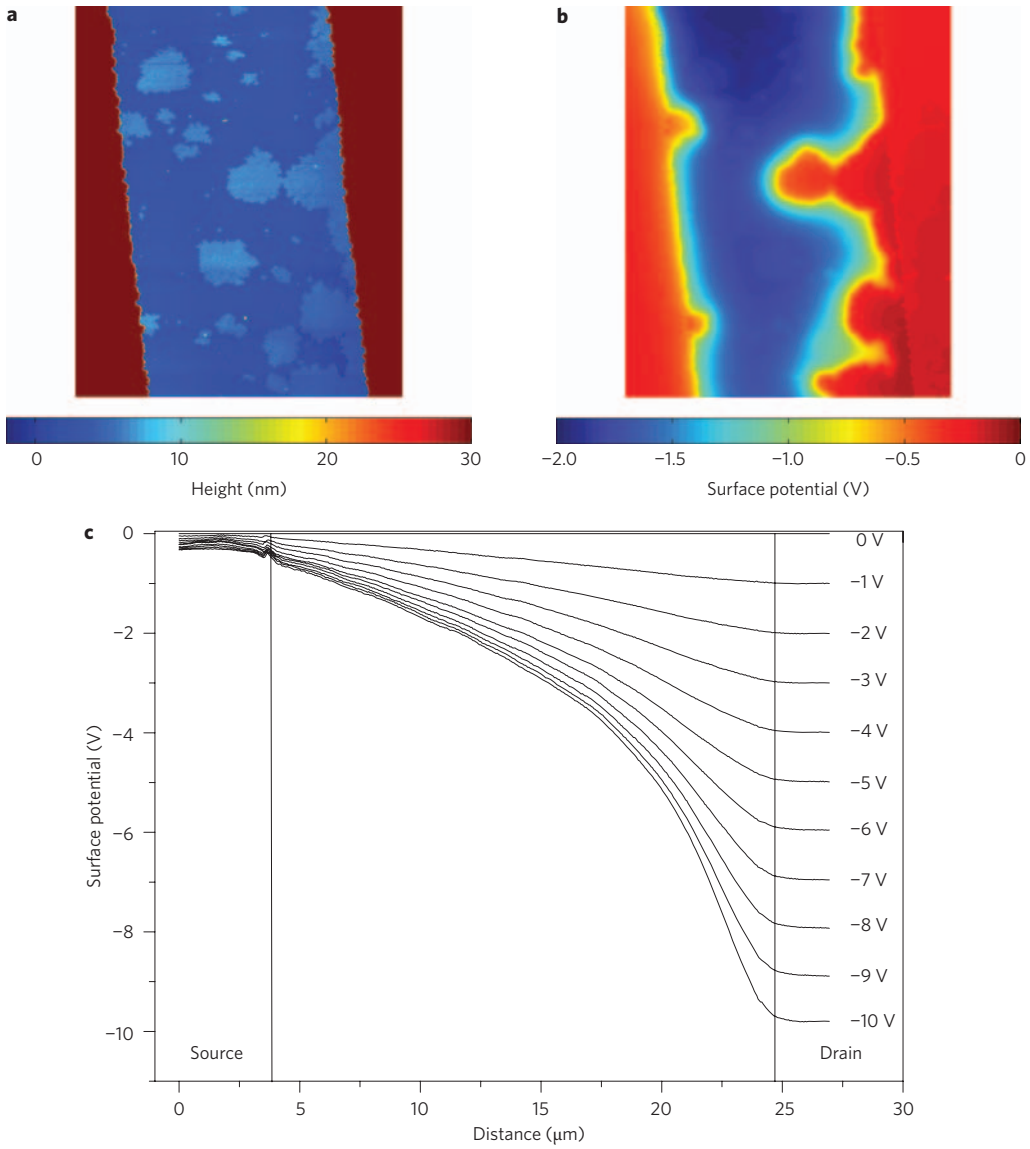

Figure 3 | Spatially resolved connectivity. a, Topography of a partially covered SAMFET measured with AFM. The dark red regions on the left and right are the gold electrodes. The channel length was 5 μm. **b**, The corresponding surface potential map measured using SKPM. The gate bias was set at −3 V and the source and drain electrodes were grounded. **c**, Surface potential profiles as measured for a fully covered SAMFET. The profiles were obtained at a drain bias ranging from 0 to −10 V in steps of −1 V with a gate bias of −5 V. The potential profile measured with the source and drain electrode grounded has been subtracted from all profiles. No additional transformations have been applied.

For efficient charge transport within the monolayer, long-range connectivity is also required. We have shown that the SAM islands grow in an ordered crystalline fashion. Electrical connectivity, however, cannot be inferred from the X-ray measurements. Preliminary scanning Kelvin probe microscopy (SKPM) measurements[9] on partially covered SAMFETs show that the only parts that contribute to the total device current are the parts in contact with both electrodes. Here, we extend these results by showing that in fully covered SAMFETs, the surface potential is smooth, indicating the absence of any electrical barrier in the channel and at the contacts.

The topography of a partially covered SAMFET is presented in Fig. 3a. The image shows islands of self-assembled molecules between the electrodes. Some islands are connected to the electrodes while others are not. The local potentials were determined using SKPM with grounded electrodes and −3 V on the gate. The spatially resolved potential map is presented in Fig. 3b. A comparison of the topography and potential shows that islands connected to one of the electrodes are at the electrode potential, 0 V. The gate field is screened by accumulated holes injected from the adjacent electrode. In islands that are electrically separated from the electrodes, the gate bias cannot be compensated and the measured potential is basically the gate potential. Consequently, there is no contrast between the disconnected islands and the bare SiO_2 gate dielectric. Therefore islands, or clusters of islands, only contribute to the total device current when they are part of a percolating path connecting both electrodes.

Obstructions in the electrical transport appear as steps in the local electrostatic potential[13]. Figure 3b suggests a minimal resistance between domains. However, to observe electrical barriers, a current has to flow. To confirm the absence of detrimental barriers at grain boundaries, the surface potential was obtained in a fully covered SAMFET (Fig. 3c). The gate bias was fixed at −5 V and the drain bias varied between 0 and −10 V. The shape evolution is identical to that measured for bulk thin-film transistors (TFTs). A detailed interpretation of SKPM data on bulk TFTs has been

presented elsewhere[14]. Here, we emphasize the smoothness of the potential. The absence of steps indicates that the SAM is homogeneously conductive. Imperfections such as grain boundaries or voids could not be identified. The electrical connection between grains, possibly with different crystallographic orientations, is therefore perfect. Note also that the surface potential is smooth even at the contacts, indicating that the contact resistance is small[13].

The absence of a significant contact resistance is remarkable in itself, because the electrodes contain a titanium adhesion layer 10 nm in thickness, which is much thicker than the SAM. Because titanium is a relatively low work-function metal, a Schottky-type contact is expected. To prevent injection-limited contacts, the electrodes were deliberately under-etched. Here, we examine the critical interface between the SAM and the electrode, in which both electrode and SAM are resolved.

The critical region where the SAM meets the edges of the electrode was imaged with transmission electron microscopy (TEM) to produce a cross-section of the SAMFET. The image in Fig. 4a describes the structure from the bottom to top of the silicon gate, the SiO_2 gate dielectric, a part of the titanium layer and the gold electrode. In the top of the image the protecting aluminium and platinum layers can be seen. The gold electrode is under-etched by about half a micrometre. The titanium layer at the edge of the contact has been dissolved by the HNO_3/HF etchant (the end of the residual titanium is indicated by the arrow). The gold electrode has collapsed and now contacts the SiO_2.

It is clear that the spatial resolution is insufficient to resolve the SAM. We therefore used energy filtered TEM to visualize the edge of the electrode. Two images were taken, one selective for carbon and one for aluminium. Figure 4b shows the combined RGB map in which carbon is presented in blue and aluminium in red. The carbon content is concentrated at the gate dielectric interface. The presence of carbon is a fingerprint of the self-assembling molecules. The carbon signal extends below the under-etched gold electrode, indicating that the SAM is also formed under the electrode, creating an intimate electrical contact. To unequivocally assign the carbon signal to the self-assembling molecules we measured the carbon and sulphur content with energy-dispersive X-ray spectroscopy. Along a cross-section at the gate dielectric interface the sulphur profile coincided with the carbon profile, unambiguously linking the carbon signal to the SAM. Therefore, we can conclude that despite the use of the titanium adhesion layer, the charge injection occurs through the gold contact, directly into the SAM.

Having established an insignificant contact resistance and that grain boundaries have a negligible effect on conductivity, we are now able to describe the charge transport through partially covered films. For incomplete monolayer transistors current can only be measured when a percolating path is present between source and drain electrodes. The existence of such a path not only depends on the coverage but also on the channel length. For a given coverage, the probability for the existence of a percolating path increases with decreasing channel length. Therefore, for intermediate coverage, the effective device mobility is expected to be a function of both coverage and channel length. This scaling relation has not yet been addressed.

Typical transfer characteristics where the drain current is plotted as a function of gate bias in the linear and saturated regime are presented in Fig. 5a–d for partially and fully covered SAMFETs. The channel length L was varied between 1 and 40 μm. From the transfer characteristics in Fig. 5b and d we can infer that the current in the fully covered SAMFET is approximately inversely proportional to channel length, that is, classic ohmic behaviour[15]. In striking contrast, Fig. 5a and c show inverse scaling for partially covered SAMFETs, that is, a huge, superlinear decrease of the drain current with increasing channel length. In fact, transistors with channel lengths larger than 7.5 μm do not show any drain current at all.

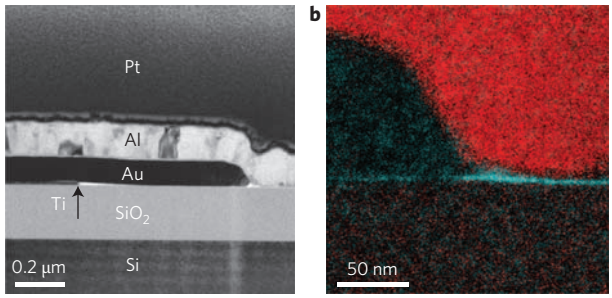

Figure 4 | Visualization of the SAM. a, Bright-field TEM image of the edge of a SAMFET electrode. The chemical composition of the layers is indicated. The image shows that the gold electrode is under-etched by about half a micrometre. The arrow indicates the end of the titanium adhesion layer. **b**, A carbon and aluminium image constructed from energy-filtered TEM measurements. Aluminium is represented in red and carbon in blue. The carbon image shows that the molecules are confined in a thin layer. The carbon signal extends below the under-etched gold electrode, which indicates that the SAM is formed under the electrode, creating an intimate electrical contact.

To quantify the channel length dependence, device mobility was extracted in the linear as well as in the saturated region. The values were comparable. The crossed and solid points in Fig. 6 show the extracted linear and saturated device mobility as a function of channel length and coverage. The fully covered SAMFET (square symbols) shows a mobility that barely depends on channel length, as is expected when contact resistances can be ignored[16]. In partially covered SAMFETs, however, the extracted device mobility collapses with channel length. In fact, within experimental accuracy the mobility decreases exponentially with channel length.

To verify the exponential dependence of the extracted device mobility as a function of channel length, we numerically calculated the current through an ensemble of conducting islands in a non-conductive matrix (inset to Fig. 6). Simulations were performed in the linear regime on a square grid of resistors. The non-conductive matrix was described by constant, high-ohmic resistors. The conducting islands were incorporated by setting the resistors in the corresponding circular areas to a low value such that the mobility obtained for the fully covered SAMFET reached 0.01 $cm^2\ V^{-1}\ s^{-1}$. Islands were added on random positions, allowing overlap, until the desired coverage was reached. A representative microstructure realized with such an ensemble of discs is presented in the inset of Fig. 6. For each channel length a voltage was applied across the resulting grid and the total conductance calculated using Kirchhoff's loop and node rules. For a given coverage and channel length, the total conductance was averaged over more than 200 different random island configurations. The average conductance did not depend on the value of the high-ohmic resistors, provided that it was orders of magnitude larger than the value of the low-ohmic resistor. Moreover, the total conductance turned out to be virtually independent of the radius of the discs. The effective device mobility as calculated for the measured coverage is presented in Fig. 6 by open symbols. A good agreement with the experimental data is obtained. Note that this implies that the resistivity per unit area in the actual SAMFET is constant for all islands, independent of their size. Consequently the exponential scaling of the extracted device mobility with channel length has been reproduced numerically. The agreement between simulated and extracted device mobility as a function of channel length and coverage links the topology of the SAM to the electrical transport measurements and quantifies the observed inverse scaling of device mobility.

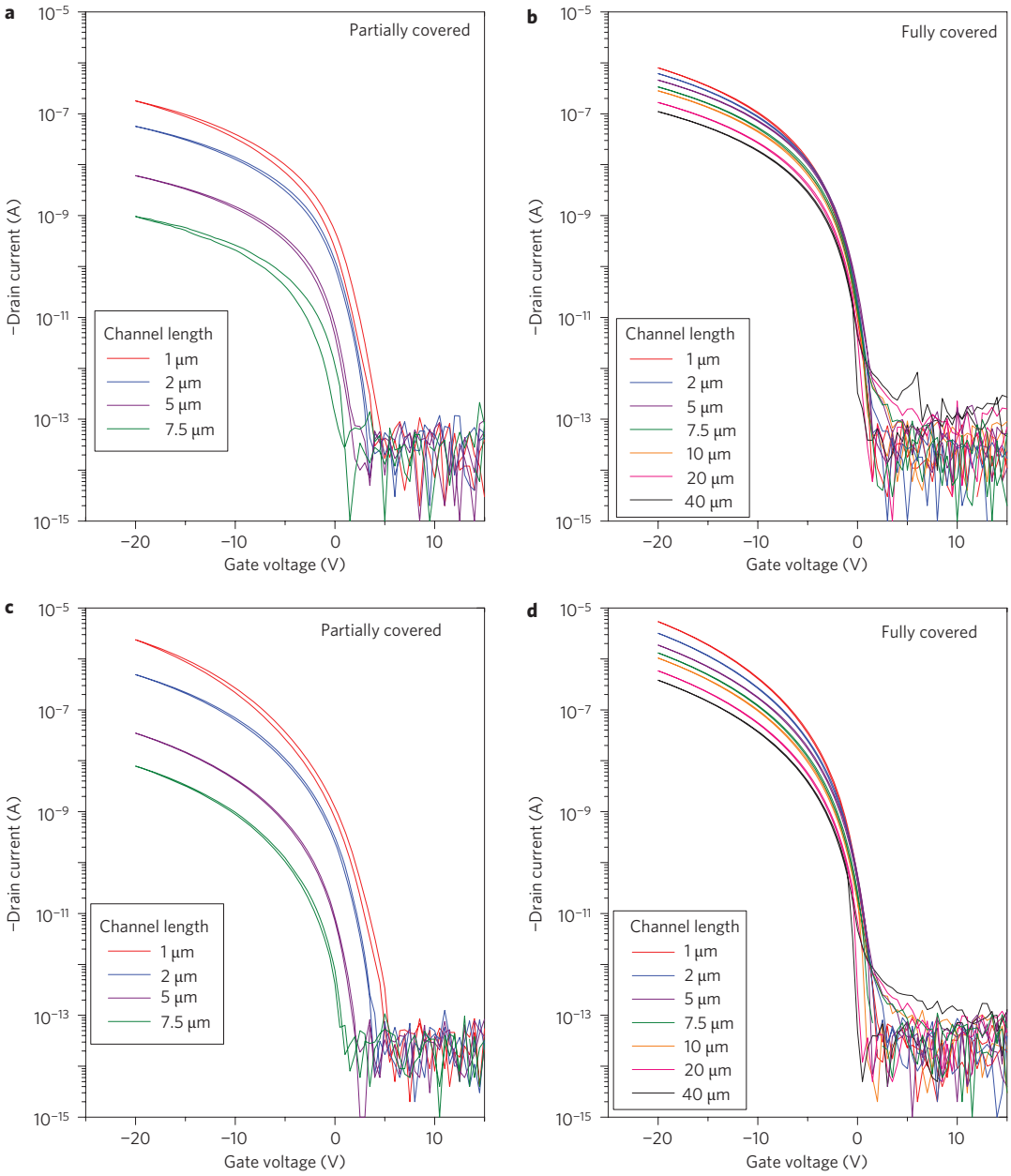

Figure 5 | Electrical transport versus monolayer coverage. a,**b**, Transfer characteristics of SAMFETs in which the drain current at a drain bias of −2 V is presented as a function of gate bias for a partially and fully covered SAMFET, respectively. **c**,**d**, The drain currents at a drain bias of −20 V. The channel length L was varied between 1 and 40 μm. Partially covered SAMFETs with channel lengths larger than 7.5 μm do not show any drain current at all.

In the following we further rationalize this exponential dependence using two approaches. The first method is based on the connectivity function. The alternative approach incorporates the measured morphology when applying a cluster radius distribution argument. Both methodologies yield an exponential scaling of mobility with channel length.

We describe the microstructure by an effective medium[17]. In this approximation the simulated SAM is disentangled and randomly redistributed over a lattice while keeping the coverage fixed. Points that are intimately connected form clusters. The probability that two individual points separated by a distance x belong to the same cluster is then given by the connectivity function $g(x)$:[18]

$$g(x) = \exp\left[-\frac{x}{\xi(p)}\right] \quad (1)$$

where the correlation length ξ is a function of the coverage p. Note that the functional dependence of ξ on p has been studied in great detail[19], but here only the exponential dependence of g on x is important. For a fully covered SAMFET the correlation length is infinite, and hence the connectivity function is unity. In this case, the source and drain electrode belong to the same and only cluster. The current is then given by[15]

$$I_{\text{complete}} = \int_0^W j_{\text{complete}} \mathrm{d}w \quad (2)$$

where j_{complete} is the current density per unit length and the integration is over the channel width W. For an incomplete SAMFET we conjecture that the major contribution to the current comes from paths connected perpendicularly between source and drain

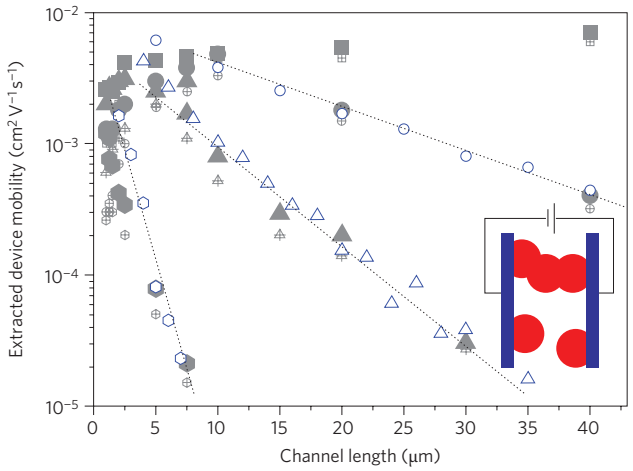

Figure 6 | Scaling of extracted linear and saturated device mobility. Crossed and filled symbols represent the extracted linear and saturated device mobility at a gate bias of −10 V as a function of channel length and coverage. The experimentally determined coverages were 0.05±0.05 (hexagons), 0.31±0.08 (triangles), 0.5±0.1 (circles) and 1 (squares). The open symbols are numerically calculated mobilities using the resistor model for SAM coverages and island sizes of 0.05 and 1.5 μm, 0.29 and 2 μm, and 0.42 and 6 μm, respectively. The dotted lines are presented as a guide to the eye and set the correlation length ξ to 2, 6 and 12 μm, respectively. The inset shows a schematic realization of an ensemble of conducting islands in a non-conductive matrix. In the actual simulation the channel width W is much bigger than its length L.

electrode. We subsequently assume that the current is proportional to the connectivity function evaluated at a distance equal to the channel length L, that is, $g(L)$. The current for the partially covered SAMFET then yields

$$I_{\text{incomplete}} = \int_0^W j_{\text{complete}} g(L)\mathrm{d}w = \exp[-L/\xi] \int_0^W j_{\text{complete}}\mathrm{d}w$$
$$= I_{\text{complete}} \exp[-L/\xi] \quad (3)$$

from which the experimentally observed dependence of I on channel length is reproduced, as shown by the dotted lines in Fig. 6. Moreover, Fig. 6 shows that the extrapolated currents at zero channel length converge to I_{complete}, as expected from equation (3). Note that an expression for the current can also be derived taking askew current paths into account. That expression cannot be solved analytically. However, numerical evaluation yielded the same exponential scaling behaviour as expected when the current is dominated by perpendicular pathways.

In the effective medium approximation, details of the microstructure are disregarded. To account for the measured morphology we used a different approach based on the distribution of cluster radii. The morphology of the SAMFET is composed of clusters, that is, ensembles of internally connected semiconducting parts. The latter are the islands shown in Figs 1 and 3. The number of clusters with radius r is given by $N(r)$. Below the percolation threshold this number is reported to depend on the radius as[20]

$$N(r) \approx \exp[-r/\xi] \quad (4)$$

When we assume that the current is proportional to the number of clusters with a radius equal to or bigger than the channel length L, we automatically find an exponential scaling with L.

In conclusion, we have unravelled the existing contradictory scaling relations in electrical transport in SAMFETs by studying the extracted device mobility as a function of channel length and monolayer coverage. In these SAMFETs, all prerequisites for efficient charge transport in a field-effect transistor are fulfilled. We observe long-range order for incomplete as well as complete SAMs together with an intimate contact between the semiconductor and electrodes. The effective device mobility for partially covered SAMFETs reproduces the dramatic, exponential decrease in mobility with increasing channel length as normally observed. This exponential scaling is a result of the coverage and is explained using percolation theory.

Partially covered SAMFETs could be well suited for use as chemical sensors. For a sensor platform, achieving ultimate mobility is not necessary. The sensitivity is dominated by the thickness of the semiconductor[21]. In fact, a partially covered SAMFET could be the ultimate sensor. Any interaction between the analyte and the SAM impairs the percolating path. In the limit of only one conducting path, the current is completely blocked.

In a broader context it should be noted that transport in inhomogeneous conductors is described by percolation. Conductivity is generally studied in a macroscopic sample where the overall conductivity is investigated as a function of the quantity of conductive material in a non-conductive matrix. Usually, the dimensions of the sample are assumed to be infinite. The uniqueness of our approach is that we explicitly take into account the microstructure by investigating the scaling of the conductivity with concentration and lateral device dimensions. In effect, we study percolation on a local instead of the more common global scale. The transport analysis performed here on partially covered SAMFETs is applicable to other percolating microelectronic systems. For instance, a comparable mobility decrease with channel length has been reported for acenes that crystallize from the contacts[22]. Our analysis could also be applied to charge transport in interpenetrating networks in co-evaporated p–n blends, graphene sheets[23], and to spatially correlated charge transport in TFTs[5]. The analysis may therefore be applicable to any percolating system showing scaling of conductance with the lateral dimensions.

Methods

Discrete SAMFETs were prepared as described previously[9]. The electrical transport was measured using an Agilent 4155C semiconductor parameter analyser. SKPM was performed using a Veeco Dimension 3100 with a Nanoscope IIIa controller operating in lift mode. First, the height profile was recorded with tapping-mode atomic force microscopy (AFM). In the second pass the potential profile was measured at a fixed lift height of 25 nm above the surface. The potential profiles were only corrected for the small offset of the $V_{sd} = 0$ V measurement. No additional transformations were applied. Cross-sections were made by means of focused ion beam transmission electron microscopy with a TECNAI F30ST TEM. A thin slab was cut from the SAMFET using focused ion beam (FIB) milling. To prevent any damage, a layer of aluminium was first deposited, followed by a layer of platinum. The thin slab was milled to electron transparency and investigated with TEM. Energy-filtered TEM was used to obtain the carbon and aluminium image. An energy-dispersive X-ray process was used to determine the carbon and sulphur profiles along the cross-sections.

Grazing incidence X-ray diffraction investigations were performed at beamline G2 at the synchrotron CHESS using radiation with a wavelength of 1.2681 Å. An angle of incidence of 0.13° was used in combination with a position-sensitive detector simultaneously covering a q_z range from 0 to 0.7 Å^{-1}.

Received 26 May 2009; accepted 1 July 2009;
published online 9 August 2009

References

1. Horowitz, G., Hajlaoui, R. & Delannoy, P. Temperature dependence of the field-effect mobility of sexithiophene. Determination of the density of traps. *J. Phys. III* **5,** 355–371 (1995).
2. Guo, X. *et al.* Chemoresponsive monolayer transistors. *Proc. Natl Acad. Sci. USA* **103,** 11452–11456 (2006).
3. Tulevski, G. S. *et al.* Attaching organic semiconductors to gate oxides: *in situ* assembly of monolayer field effect transistors. *J. Am. Chem. Soc.* **126,** 15048–15050 (2004).
4. Mottaghi, M. *et al.* Low-operating-voltage organic transistors made of bifunctional self-assembled monolayers. *Adv. Funct. Mater.* **17,** 597–604 (2007).

5. Dinelli, F. *et al.* Spatially correlated charge transport in organic thin film transistors. *Phys. Rev. Lett.* **92,** 116802 (2004).
6. Ruiz, R., Papadimitratos, A., Mayer, A. C. & Malliaras, G. G. Thickness dependence of mobility in pentacene thin-film transistors. *Adv. Mater.* **17,** 1795–1798 (2005).
7. Park, B.-N., Seo, S. & Evans, P. G. Channel formation in single-monolayer pentacene thin film transistors. *J. Phys. D* **40,** 3506–3511 (2007).
8. Whitesides, G. M. & Grzybowski, B. Self-assembly at all scales. *Science* **295,** 2418–2421 (2002).
9. Smits, E. C. P. *et al.* Bottom-up organic integrated circuits. *Nature* **455,** 956–959 (2008).
10. Yang G. & Liu, G.-Y. New insights for self-assembled monolayers of organothiols on Au(111) revealed by scanning tunneling microscopy. *J. Phys. Chem. B* **107,** 8746–8759 (2003).
11. Onclin, S., Ravoo, B. J. & Reinhoudt, D. N. Engineering silicon oxide surfaces using self-assembled monolayers. *Angew. Chem. Int. Ed.* **44,** 6282–6304 (2005).
12. Yoneda, Y. Anomalous surface reflection of X-rays. *Phys. Rev.* **131,** 2010–2013 (1963).
13. Puntambekar, K. P., Pesavento, P. V. & Frisbie, C. D. Surface potential profiling and contact resistance measurements on operating pentacene thin-film transistors by Kelvin probe force microscopy. *Appl. Phys. Lett.* **83,** 5539–5541 (2003).
14. Smits, E. C. P. *et al.* Unified description of potential profiles and electrical transport in unipolar and ambipolar organic field-effect transistors. *Phys. Rev. B* **76,** 125202 (2007).
15. Sze, S. M. *Physics of Semiconductor Devices* 2nd edn (Wiley, 1981).
16. Meijer, E. J. *et al.* Scaling behavior and parasitic series resistance in disordered organic field-effect transistors. *Appl. Phys. Lett.* **82,** 4576–4578 (2003).
17. Kirkpatrick, S. Percolation and conduction. *Rev. Mod. Phys.* **45,** 574–588 (1973).
18. Grimmett, G. *Percolation* (Springer-Verlag, 1989).
19. Stauffer, D. & Aharony, A. *Introduction to Percolation Theory* (CRC Press, 1985).
20. Stauffer, D. Speculations on the cluster radius below the percolation threshold. *Z. Physik B* **30,** 173–176 (1978).
21. Huang, J., Sun, J. & Katz, H. E. Monolayer-dimensional 5,5′-*bis*(4-hexylphenyl)-2,2′-bithiophene transistors and chemically responsive heterostructures. *Adv. Mater.* **20,** 2567–2572 (2008).
22. Gundlach, D. J. *et al.* Contact-induced crystallinity for high-performance soluble acene-based transistors and circuits. *Nature Mater.* **7,** 216–221 (2008).
23. Dato, A., Radmilovic, V., Lee, Z., Phillips, J. & Frenklach, M. Substrate-free gas-phase synthesis of graphene sheets. *Nano Lett.* **8,** 2012–2016 (2008).

Acknowledgements

The authors acknowledge financial support from the Dutch Technology Foundation STW, the EU project ONE-P (no. 212311), the Austrian Nanoinitiative and H. C. Starck GmbH. We thank M. Kaiser for FIB-TEM imaging. We thank the Cornell High Energy Synchrotron Source for provision of synchrotron radiation facilities and D. Smilgies for his assistance in using beamline G2.

Author contributions

S.M., E.S., P.H., P.B. M.K., R.J. and D.L. conceived and designed the experiments. S.M., E.S., P.H., H.W., A.M., R.R. and M.K. performed the experiments. S.P. synthesized the materials. All authors discussed the results, commented on the manuscript and co-wrote the paper.

Additional information

Supplementary information accompanies this paper at www.nature.com/naturenanotechnology. Reprints and permission information is available online at http://npg.nature.com/reprintsandpermissions/. Correspondence and requests for materials should be addressed to D.L.